Structural Chemistry (2023) 34:2347–2364
https://doi.org/10.1007/s11224-023-02151-x

RESEARCH

Electronic effects of the substituted dopants on stability and reactivity of difuranosilapyridine-4-ylidenes: DFT approach

Marziyeh Mohammadi[1]

Received: 20 November 2022 / Accepted: 20 February 2023 / Published online: 17 April 2023

Abstract

Following our quest for *N*-heterocyclic Hammick silylenes, we have to probe the electronegative and electropositive substitutions on the singlet (*s*) and triplet (*t*) silapyridine-4-ylidene fused by two furan rings compared to the synthesized silylenes by West (**I-s**), Denk (**II-s**), and Kira (**III-s**). In all cases, *s* silapyridine-4-ylidenes emerge as ground state, revealing more stability than their corresponding *t* analogous. All species seem to have a minimum on their energy surfaces, demonstrating the positive force constant and the positive frequency. The optimized *s* silylenes show bond length, divalent and dihedral bond angles, somewhat similar to their corresponding *t* congeners. Irrespective of how substituent groups are arranged in either the "W (*ortho*)" or "chair (*para*)" positions of the silylenic center, the most stability is verified by the substitution of more electronegative NH and O groups (as electron withdrawing groups; EWGs) in the corresponding furan rings, while the least stability is respected by **III-s**. In contradiction to previous reports on the *N*-heterocyclic Hammick carbenes, silylenes, and germylenes (NHCs, NHSis, and NHGes) that size, type, and orientation, in addition to the number of fused rings, formulated influence on $\Delta E_{s\text{-}t}$, $\Delta E_{HOMO\text{-}LUMO}$, and reactivity of the corresponding divalent species, now PH, AsH, S, and Se (as σ and π- electron donating groups; EDGs) similar to EWGs stabilize their silylenic derivatives. In going from second row to third row and from third row to forth row of every group in the periodic table, stability is decreased. As a result, the stability and electronic properties of *s* and *t* NHSis are considerably dependent on the electronegativity and radius of the substituted dopants.

Keywords Silapyridine · "W" or "chair" position · Silylenic center · Furan ring

Introduction

The chemistry of divalent compounds such as carbenes, organosilicon, etc. has fascinated a considerable attention in recent years [1–15]. Divalent silylenes are congeners of carbenes, but mostly seem to have the *s* configuration as the ground state [1–15]. The larger size of the valence orbitals of silicon reduces the electron–electron repulsion of the lone pair on the Si atom accordingly enlarges the split energy of electrons. Thus, a silylene energetically favors the *s* ground state as a stable configuration [1–15]. These intermediates are employed in light-emitting diode, electroluminescence, Si chemical vapor deposition procedures, optics, electronics, and semiconductors [1–15]. The simplest, acyclic, linear, and unsaturated silylene with $H_2C=Si$ molecular structure has been of great interest as a possible divalent intermediate in numerous organosilicon reactions. It may be established in the interstellar medium [1–15]. Silylidenes have been the subject of various theoretical investigations and experimental surveys [16–20]. The first unsaturated silylene was searched by Murrell et al. in 1977 at theoretical methods and levels [21]. The experimental findings recognized silylidene via its electronic absorption spectrum, in 1979 [22] and later its microwave spectrum [23]. Optical properties, structural parameters, rotational constants, force constants, and vibrational frequencies of silavinylidene derivatives were estimated using computational chemistry [24–27]. In 1997, laser-induced fluorescence spectroscopy and theoretical expectations were used in order to establish the ground state of this divalent species [28]. The influences of the substituted polar groups on thermodynamic stability ($\Delta E_{s\text{-}t}$) were first described by Hopkinson et al. [29]. In spite of many investigations, achieving at *s* ($\Delta E_{s\text{-}t} > 0$) vs. *t* ground state ($\Delta E_{s\text{-}t} < 0$) for saturated and unsaturated NHCs, NHSis, and NHGes seems as a challenging issue.

✉ Marziyeh Mohammadi
m.mohammadi@vru.ac.ir

[1] Department of Chemistry, Faculty of Science, Vali-e-Asr University of Rafsanjan, Rafsanjan, Iran

If the promotion energy is increased, the *s* ground state will be reached. If the promotion energy is decreased, the *t* ground state will be reached. To this end, electronic, inductive, mesomeric, and steric influences are applied to change the multiplicity of NHCs, NHSis, and NHGes [29–34]. For instance, the substituted EDGs increase the 3p-character of Si valence orbitals which leads to *t* configuration. Gordon identified the first *t* ground state silylenes [17, 18, 30]. Apeloig researched the effects of EDGs on the multiplicity of silylenes [19, 20, 31]. Considering applications of unsaturated silylenes and increasing demand for stable NHSis [34], here we have studied substituent effects of EWGs and EDGs on two "W" and "chair" orientations with silylenic centers of **1-s**, **2x-s**, **3x-s**, and **1-t**, **2x-t**, and **3x-t** Hammick silylenes (*x*=NH, PH, AsH, O, S, and Se), at DFT (Fig. 1) [35–39].

Computational methods

Geometry optimizations are carried out without any symmetry constraint, operating the GAMESS [40, 41] program at the (U)B3LYP [42–45] and (U)M06-2X methods [46, 47] together with 6–311 + + G** and AUG-cc-pVTZ basis sets [48–55]. All optimized structures turn out to be minima on their energy surfaces for showing no imaginary frequency. The *s-t* energy gap ($\Delta E_{s\text{-}t}$), energies of the frontier molecular orbital (FMO), band gap ($\Delta E_{\text{HOMO-LUMO}}$ and $\Delta E_{\text{SOMO-SOMO+1}}$ for *s* and *t* species, respectively), ionization potential (IP), and electron affinity (EA) are calculated at 298.15 K and 1.00 atm [56–79]. The natural bond orbital (NBO) charges [56–59], the global reactivity descriptors [80–83], and the condensed Fukui function (CFF) are provided at the same level of theory [84, 85]. The nucleophilicity index (*N*) is acquired from the energy difference between E_{HOMO} of *s* NHSi (or E_{SOMO} of *t* NHSi) and tetracyanoethylene [80–83]. The electrophilicity index ($\omega=\mu^2/2\eta$), chemical potential ($\mu=(E_{\text{HOMO}}\text{-}E_{\text{LUMO}})/2$), and the maximum amount of electronic charge index ($\Delta N_{\max}=-\mu/\eta$)are obtained as well [80–83]. The CFF descriptors are calculated using the Multiwfn program via $f^+{}_A=\rho^A{}_{N+1}-\rho^A{}_N$ (ρ^A is the electron population number of *A* atom and *N* refers to the number of electrons stable states), $f^+{}_A=q^A{}_{N+1}-q^A{}_N$ (nucleophilic attack), $f^-{}_A=q^A{}_N-q^A{}_{N-1}$ (electrophilic attack), and $DfA=f^+A-f^-A$ (condensed dual descriptor) [84, 85]. The site is favored for a nucleophilic attack if $DfA>0$ and is favored for an electrophilic attack if $DfA<0$.

Results and discussion

Following the previous research works on divalent compounds [34–39], in this research the substitution effects were studied on the singlet (s) and triplet (t) silapyridine-4-ylidene fused by two furan rings. The physical prarmeters have been obtained using DFT calculations according to the previous reports [60–79]. The present work covers thermodynamic, kinetic, and electronic effects of EWGs and EDGs on the scrutinized *s* and *t* NHSis vs. the first synthesized silylenes at DFT (Schemes 1) [86–89].

Recently, different theoretical studies has been carried out on fusion of the different rings of pyridine-4-ylidene and heavier derivatives (Schemes 2).

The resulted reports reveal that heteroatom type, size of the fused ring, number of fused rings, and orientation of the substituted dopants change stability and other properties of these divalent species. Our *s* and *t* NHSis turn out to be minima for showing no negative force constant. Structural parameters including bond length (R; C—Si and Si—C) in angstrom, divalent and dihedral bond angles in degree ($\hat{A}$ (C − Si − C) and $\hat{D}$ (C − Si − C − X), respectively), and symmetry of silylenes are considered. Except for **3AsH-s** and **3PH-s** with C_1 symmetry, structural optimizations of other silylenes show C_s symmetry for all *s* and *t* states. All silylenes show $\hat{D}\cong 180°$. In each of the three series, **1-s**, **2x-s**, and **3x-s** silylenes show more *R* (about 0.020–0.040 Å) and less $\hat{A}$ (about 10°) than their **1-t**, **2x-t**, and **3x-t** analogous. For instance, **2O-s** and **3AsH-s** show *R* of 1.868, 1.890, 1.853, and 1.846 Å, also $\hat{A}$ of 92.461° and 94.434°, respectively. Likewise, **2O-t** and **3AsH-t** show *R* of 1.878, 1.876, 1.864, and 1.836 Å, also $\hat{A}$ of 102.021° and 104.150°, respectively. Our silylenes turn out as singlet ground state for showing positive $\Delta E_{s\text{-}t}$ values [33]. In series 1, while fusion of two benzene rings thermodynamically stabilizes the corresponding silylene ($\Delta E_{s\text{-}t}=185.30$ kJ/mol), in series 2 and 3, by decreasing the electronegativity and increasing the atomic radius, the $\Delta E_{s\text{-}t}$ diminishes from 215.10 kJ/mol for EWGs to 193.66 kJ/mol for EDGs (Table 1).

All silylenes show more $\Delta E_{s\text{-}t}$ than **III** (138.48 kJ/mol). This is because of the higher electronegativity of EWGs which makes them a stronger π-acceptor and hence prefers the singlet over the triplet state which causes a higher $\Delta E_{s\text{-}t}$. In going from the most electronegative heteroatom to the least electronegative one, the $\Delta E_{s\text{-}t}$ is decreased. More π-electron delocalization of the substituted dopant's free electron pair in two furan rings and a silapyridine ring makes possible more polarity and less polarizability of the *s* NHSis with regard to the *t* ones. Then again, substitution of either EWGs or EDGs groups in a zigzag (W) arrangement to the silylenic center produces less polarity. In accordance with Hoffmann et al.'s statement [89], a molecule could be known as stable if its smallest vibrational frequency is at least 100 cm^{-1} and it reveals an enormous FMO energy difference (here $\Delta E_{\text{HOMO-LUMO}}$ for *s* states and $\Delta E_{\text{SOMO-SOMO+1}}$ for *t* ones) [86–88]. Now, vibrational analysis demonstrates that the scrutinized NHSis including **1-s**, **2x-s**, **3x-s**, **1-t**, **2x-t**, and **3x-t**, where *x*=NH, PH, AsH, O, S, and Se, are real minimums revealing positive frequency, and hence positive force constant (Table 2).

While fusion of two benzene rings kinetically stabilizes the *s* and *t* states of the corresponding silylenes, **1-s** ($\Delta E_{\text{HOMO-LUMO}}=364.96$ kJ/mol) and **1-t**

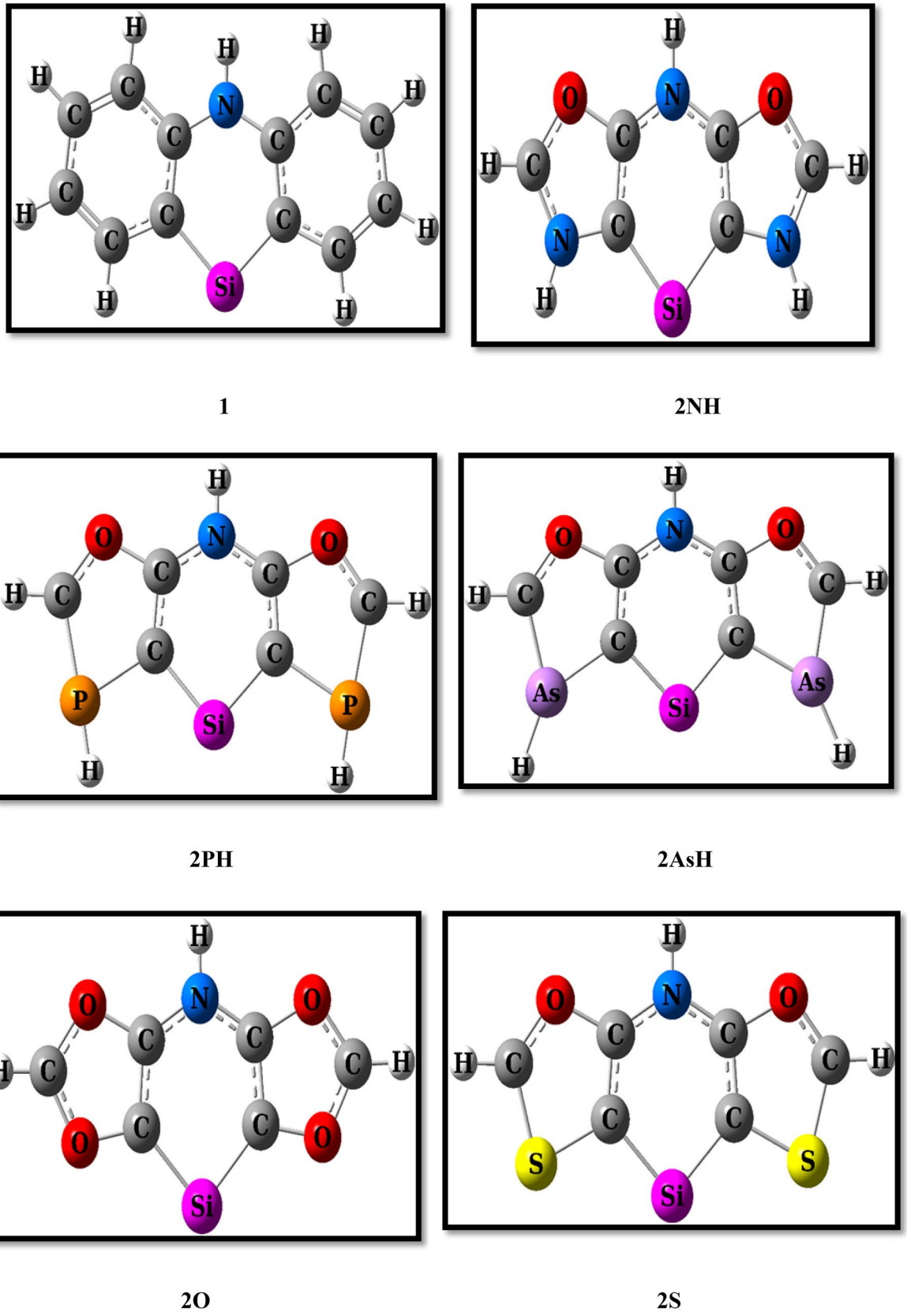

Fig. 1 The optimized structures of the studied NHSis in this work

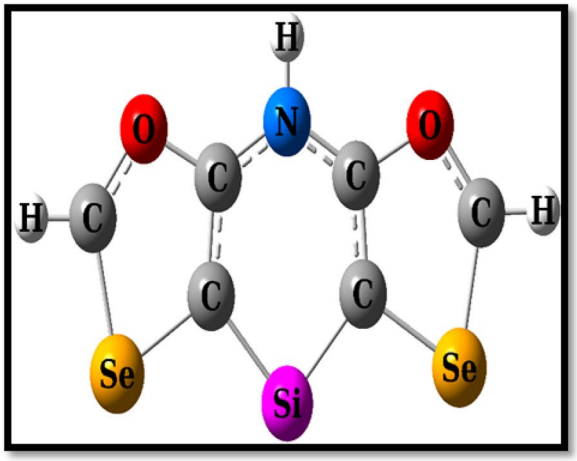

2Se

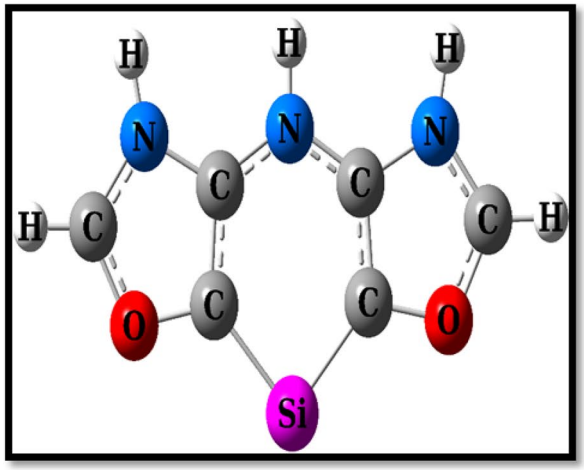

3NH

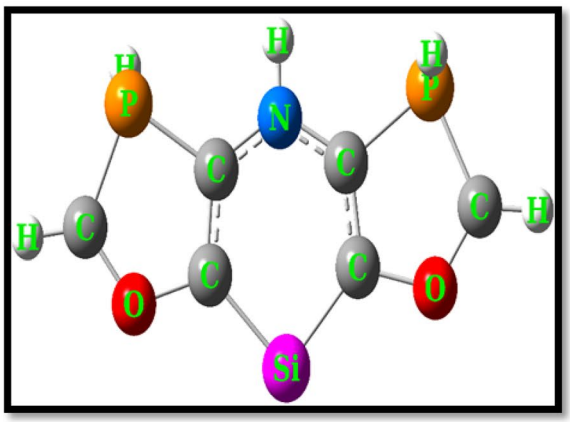

3PH

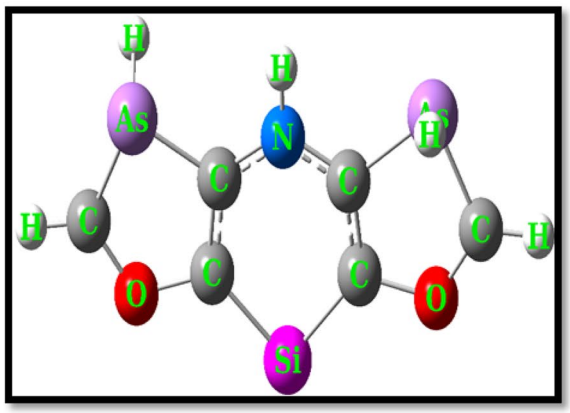

3AsH

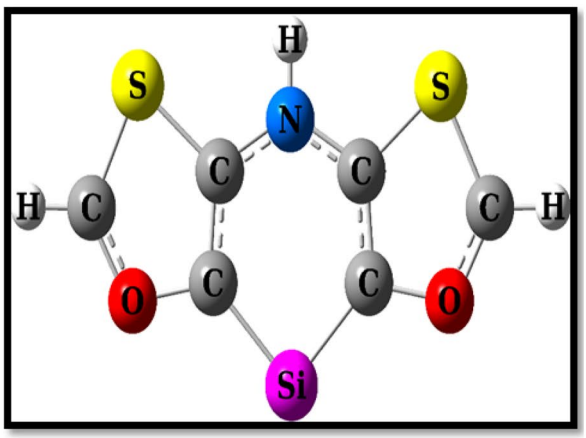

3S

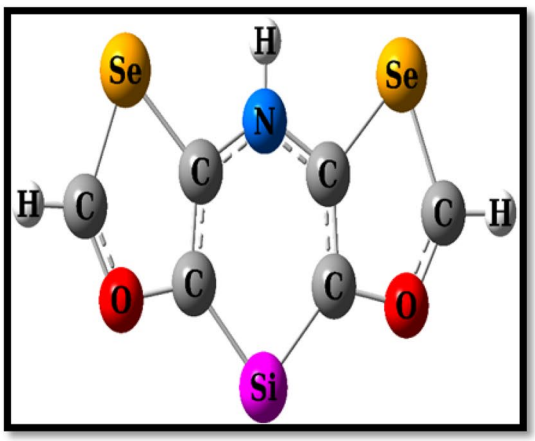

3Se

Fig. 1 (continued)

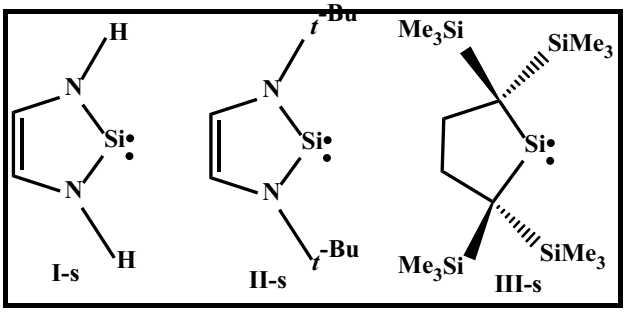

Scheme 1 Thesynthesized silylene by West (**I-s**),Denk (**II-s**) as well asKira (**III-s**)

($\Delta E_{\text{SOMO-SOMO+1}} = 290.09$ kJ/mol), in two other series by decreasing the electronegativity of *x* dopants and increasing their atomic radius, the kinetic stability is diminished from 393.46 for EWGs to 191.61 kJ/mol for EDGs (Table 2). Hence, amid *s* NHSis, the most kinetic stable structures are **2NH-s** and **2O-s** (393.38 and 393.46 kJ/mol), and the least stable ones are **3PH-s** and **3AsH-s** (378.04 and 379.50 kJ/mol), correspondingly, which they are stabilized considerably more than **IIIs** (351.33 kJ/mol). Between *t* NHSis, **2NH-t** and **2O-t** species to some extent accomplish the abovementioned conditions by Hoffmann et al., indicating the smallest vibrational frequency of 73.42 and 73.57 cm^{-1} besides $\Delta E_{\text{SOMO-SOMO+1}}$ of 299.92 and 277.68 kJ/mol respectively. Between *t* NHSis, **3AsH-t** species contravene the above conditions, emerging lower vibrational frequency of 66.96 cm^{-1} and a lower $\Delta E_{\text{SOMO-SOMO+1}}$ (191.61 kJ/mol) than that of the distinguished by Hoffmann and co-workers. The band gap of all *s* and *t* NHSis is more than **III-s** ($\Delta E_{\text{HOMO-LUMO}} = 351.33$ kJ/mol) and **III-t** ($\Delta E_{\text{SOMO-SOMO+1}} = 138.32$ kJ/mol). Among these synthesized silylenes, the silylenic centers of **I-s** and **II-s** molecules completely enjoy from π-conjugation of two nitrogen groups adjacent to their silylenic centers, while **III-s** benefits only from the hyper-conjugation effect of four $SiMe_3$ groups. This difference significantly is influenced on stability of them. Here, the optimized NHSis similar to **III** silylene suffer from lack of π-donating of the neighboring nitrogen groups to silylenic centers. The highest occupied molecular orbital (HOMO) and the lowest unoccupied molecular orbital (LUMO) of *s* NHSis is considered dissimilar to the semi occupied molecular orbital (SOMO, SOMO + 1) of *t* NHSis (for instance, **2O-s** and **2O-t** silylenes, Fig. 2).

Replacement of two EWGs in chair organizations to the silylenic center of **2O-s** progresses unbroken π-conjugation by employing $3\sigma^2$ or sp^2—lone pair of the divalent center and reduces HOMO energy of **1-s** from −520.13 to −581.25 kJ/mol in **2O-s** and hence increases stability of HOMO of **2O-s** structure. Undoubtedly, conjugation of the free electron pairs on EWGs with π-electrons of the fused double bond (C = C) in the silapyridine ring of **2O-s** structure, decreases LUMO energy of **1-s** from −155.28 to −187.80 kJ/mol in **2O-s** (Fig. 2). Moreover, conjugation of the unpaired lone pairs on EWGs with the semi-filled $3p_\pi$-orbital of the silylenic center of **2O-t** diminishes the SOMO energy of **1-t** from −322.10 to −354.89 kJ/mol in **2O-t** and henceforth increases the stability of SOMO in **2O-t**. Furthermore, replacement of two EWGs in chair positions to the silylenic center of the **2O-t** structure adjusts π-conjugation by employing the

Scheme 2 The reported newly divalent species in the computational chemistry

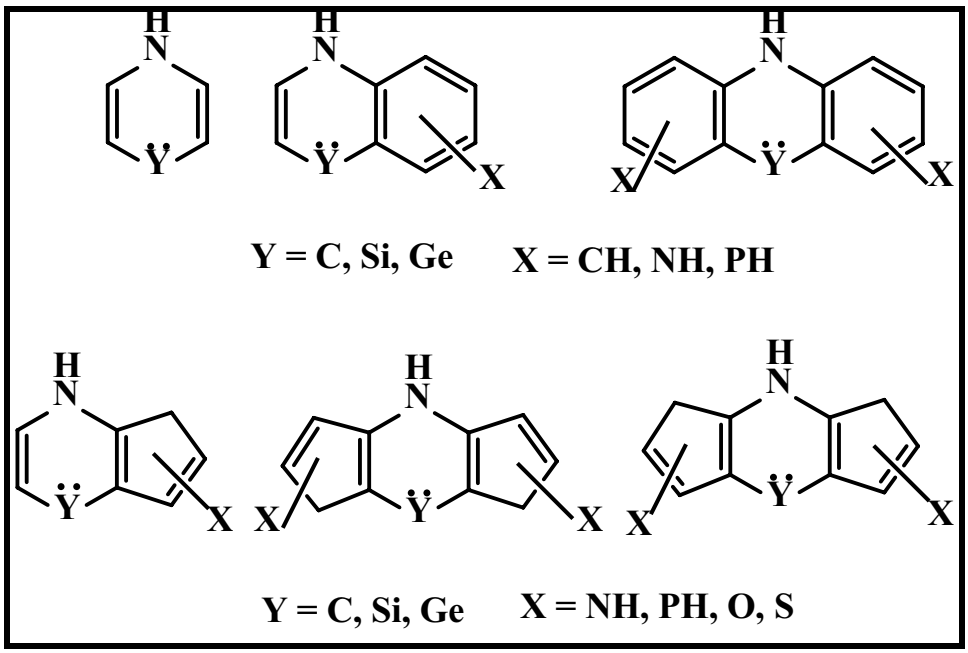

Table 1 The calculated $\Delta E_{s\text{-}t}$ (in kJ/mol), polarity (in Debye), and polarizability (in kJ/mol) of the inspected singlet and triplet NHSis

Species	$\Delta E_{s\text{-}t}$	Polarity	Polarizability
1-s	185.30	4.77	309,407.70
1-t		2.27	308,696.12
2NH-s	213.18	2.03	300,763.26
2NH-t		1.12	314,362.44
2PH-s	205.11	2.20	350,811.41
2PH-t		1.07	367,520.48
2AsH-s	204.69	2.36	367,810.38
2AsH-t		1.04	386,496.08
2O-s	215.10	3.50	281,286.92
2O-t		1.52	295,782.17
2S-s	205.91	3.22	323,797.53
2S-t		1.11	341,429.03
2Se-s	204.74	3.16	341,139.12
2Se-t		0.95	364,700.49
3NH-s	212.72	8.27	299,155.61
3NH-t		6.09	305,085.48
3PH-s	195.04	7.28	360,510.05
3PH-t		5.35	361,195.28
3AsH-s	193.66	6.92	379,960.04
3AsH-t		5.04	388,841.67
3S-s	197.46	5.67	330,175.44
3S-t		3.77	331,308.71
3Se-s	196.79	5.64	352,550.84
3Se-t		3.78	352,445.42
I-s	258.49	1.61	211,367.10
I-t		3.92	229,367.57
II-s	224.63	1.28	230,342.70
II-t		3.34	250,715.12
III-s	138.48	1.15	283,158.12
III-t		0.90	293,146.67

Table 2 The rounded frequency (in cm^{-1}), FMO energy (in kJ/mol), and their energy differences ($\Delta E_{HOMO-LUMO}$ for *s* states and $\Delta E_{SOMO-SOMO+1}$ for *t* ones in kJ/mol) of the inspected singlet and triplet NHSis

Species	Frequency	E_{HOMO} (α-E_{SOMO})	E_{LUMO} (α-E_{SOMO+1})	$\Delta E_{HOMO\text{-}LUMO}$ (α-$\Delta E_{SOMO\text{-}SOMO+1}$)
1-s	132.00	−520.13	−155.28	364.96
1-t	43.00	−322.10	−32.00	290.09
2NH-s	185.00	−557.11	−163.67	393.38
2NH-t	74.00	−328.66	−28.59	299.92
2PH-s	150.00	−556.85	−172.85	384.06
2PH-t	55.00	−336.26	−91.02	245.07
2AsH-s	146.00	−556.59	−173.11	383.43
2AsH-t	67.00	−334.95	−108.33	226.56
2O-s	174.00	−581.25	−187.80	393.46
2O-t	74.00	−354.89	−77.11	277.68
2S-s	169.00	−573.90	−189.64	384.27
2S-t	59.00	−352.79	−123.02	229.90
2Se-s	185.00	−569.70	−188.59	381.26
2Se-t	62.00	−349.38	−132.98	216.48
3NH-s	182.00	−539.02	−150.30	388.53
3NH-t	74.00	−322.10	−74.49	247.79
3PH-s	137.00	−537.97	−160.26	378.04
3PH-t	70.00	−331.54	−92.07	239.39
3AsH-s	144.00	−538.49	−158.95	379.50
3AsH-t	67.00	−330.75	−139.02	191.61
3S-s	152.00	−560.52	−177.84	382.60
3S-t	42.00	−350.43	−119.61	230.95
3Se-s	172.00	−557.38	−174.43	382.93
3Se-t	40.00	−347.02	−129.05	217.90
I-s	375.10	−526.69	−75.28	451.48
I-t	69.33	−320.79	−59.54	261.29
II-s	361.09	−496.52	−65.84	430.71
II-t	55.62	−265.44	−50.10	215.35
III-s	362.39	−535.34	−184.13	351.33
III-t	61.72	−322.36	−184.13	138.32

half-captured s^1p^1 orbital of the silylenic center and free electrons of furan's oxygen and hence reduces SOMO + 1 energy of **1-t** from −32.00 to −77.11 kJ/mol then increases stability of SOMO + 1 in **2O-t** (Fig. 2). Delocalization of free electron pairs on EDGs and oxygen heteroatoms in the silapyridine ring not only leads to low leveling of HOMO and SOMO (e.g., from −520.13 in **1-s** to −538.49 kJ/mol in **3AsH-s** and from −322.10 in **1-t** to −330.75 kJ/mol in **3AsH-t**) but also delocalization in the fused furan rings changes LUMO and SOMO + 1 energy (e.g., from −155.28 in **1-s** to −158.95 kJ/mol in **3AsH-s** and from −32.00 in **1-t** to −139.02 kJ/mol in **3AsH-t**, Fig. 3).

Interestingly, the presence of two EWGs in the fused furan rings either in the "W" or "chair" positions of the silylenic center of the *s* and *t* NHSis engages π-cross conjugation (β-SOMO + 1 in **2O-t**, Fig. 2) and the resulted ring current of the silapyridine ring has more than two EDGs. The polarity and polarizability of *s* NHSis with the substituted EWGs are different from those of *s* NHSis with the substituted EDGs and even the corresponding *t* ones. This observation implies that besides the inductive effect of more electronegative elements, by involving lone pairs of the substituted groups and silylenic centers in mesomeric effect, and π-conjugation polarity is decreased due to the increment of ring current with respect to chair arrangement to silylenic center (Table 2). Consistent with the DOS plots, every *s* NHSi displays more E_g value than its corresponding *t* NHSi so that the most value is estimated for the substituted EWG—singlet silylenes, and the least value is calculated for the substituted EDG—triplet silylenes. For example, 4.00 eV for **2O-s** vs. 2.56 eV for **2O-t** (Fig. 4), also 3.94 eV for **3AsH-s** vs. 1.99 eV for **3AsH-t** (Fig. 5).

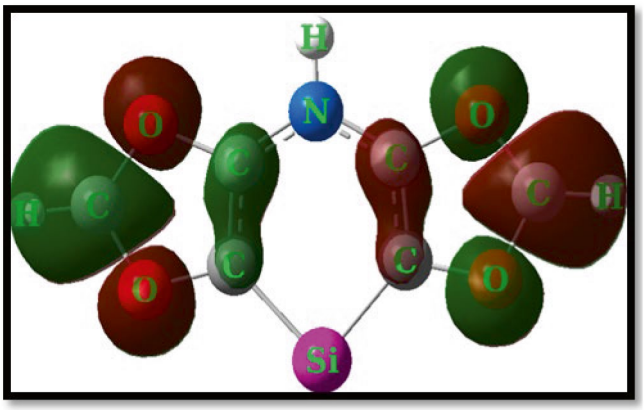

2O-s; HOMO

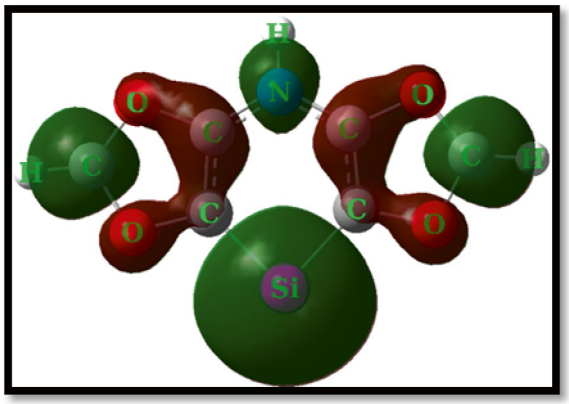

2O-s; LUMO

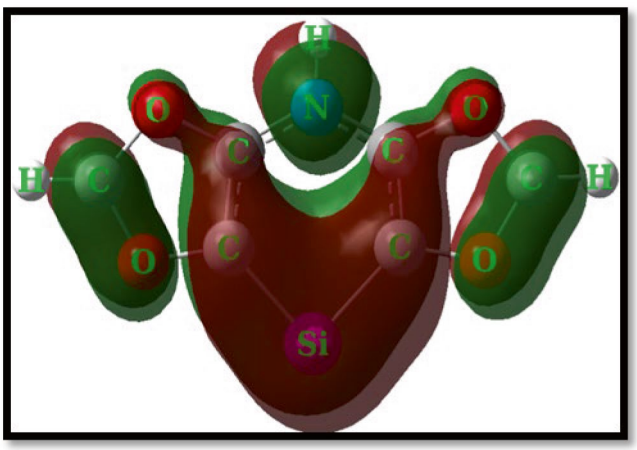

2O-t; α-SOMO

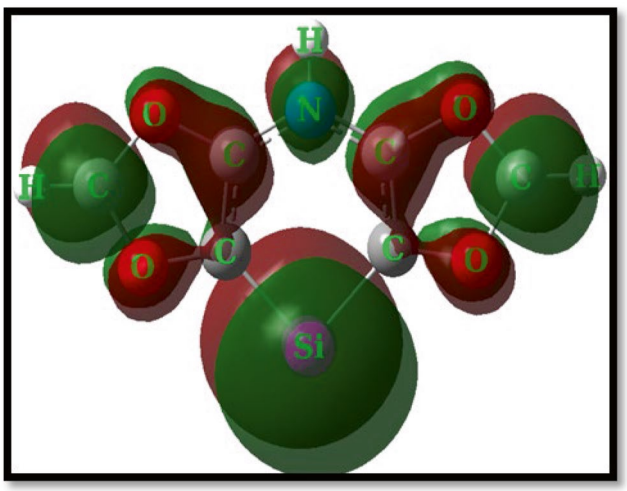

2O-t; α-SOMO+1

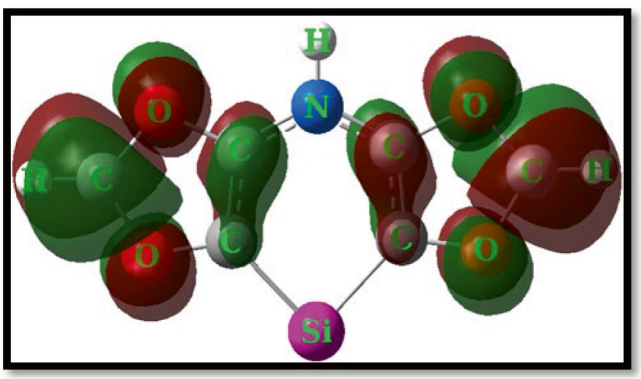

2O-t; β-SOMO

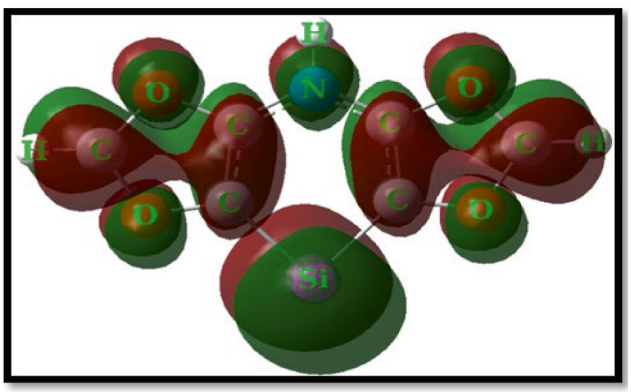

2O-t; β-SOMO+1

Fig. 2 The FMO shapes of the selected **2O-s** and **2O-t** silylenes

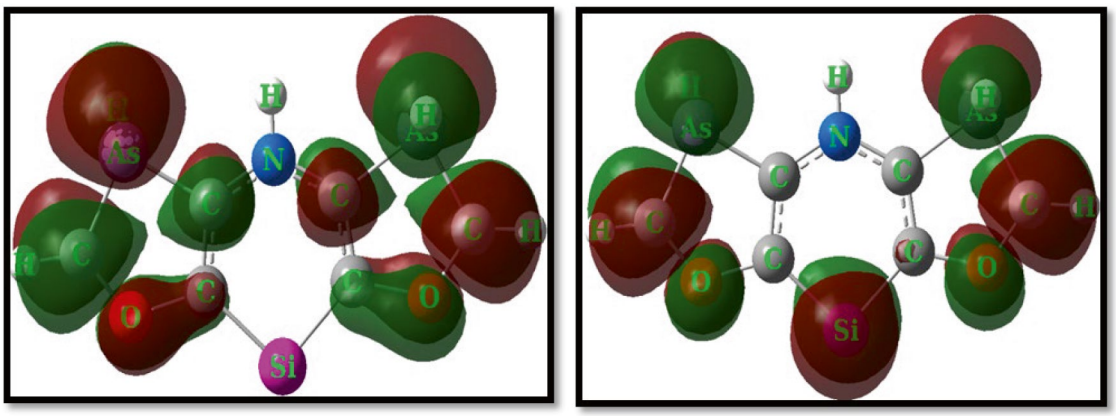

3AsH-s; HOMO 3AsH-s; LUMO

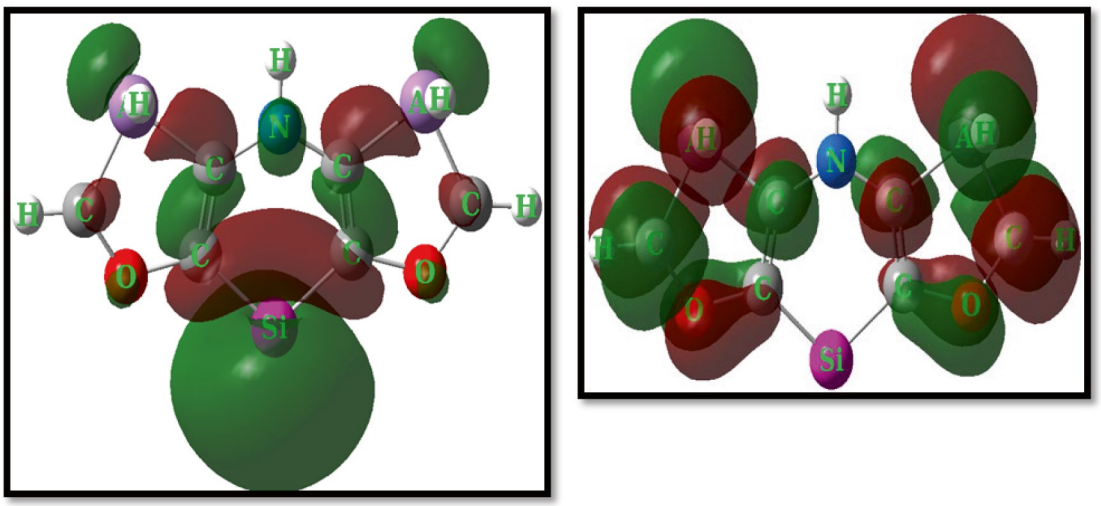

3AsH-t; α-SOMO 3AsH-t; α-SOMO+1

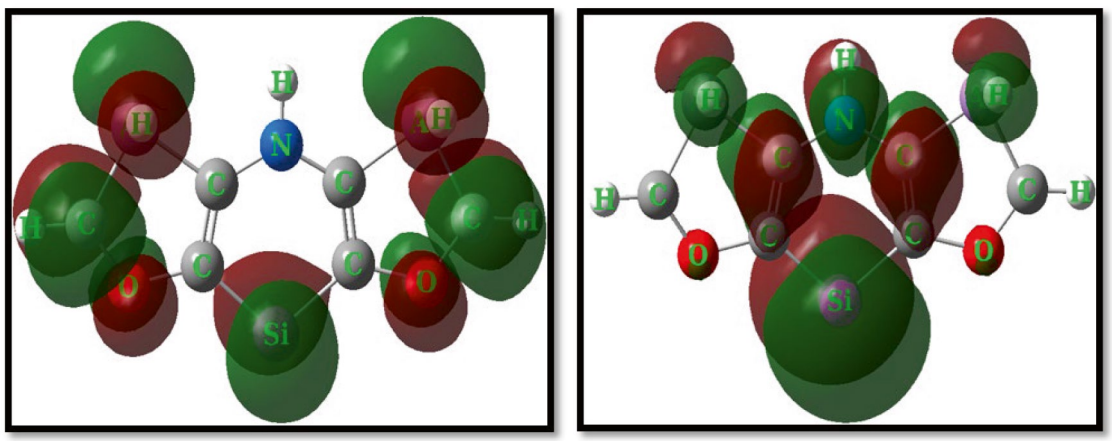

3AsH-t; β-SOMO 3AsH-t; β-SOMO+1

Fig. 3 The FMO shapes of the selected **3AsH-s** and **3AsH-t** silylenes

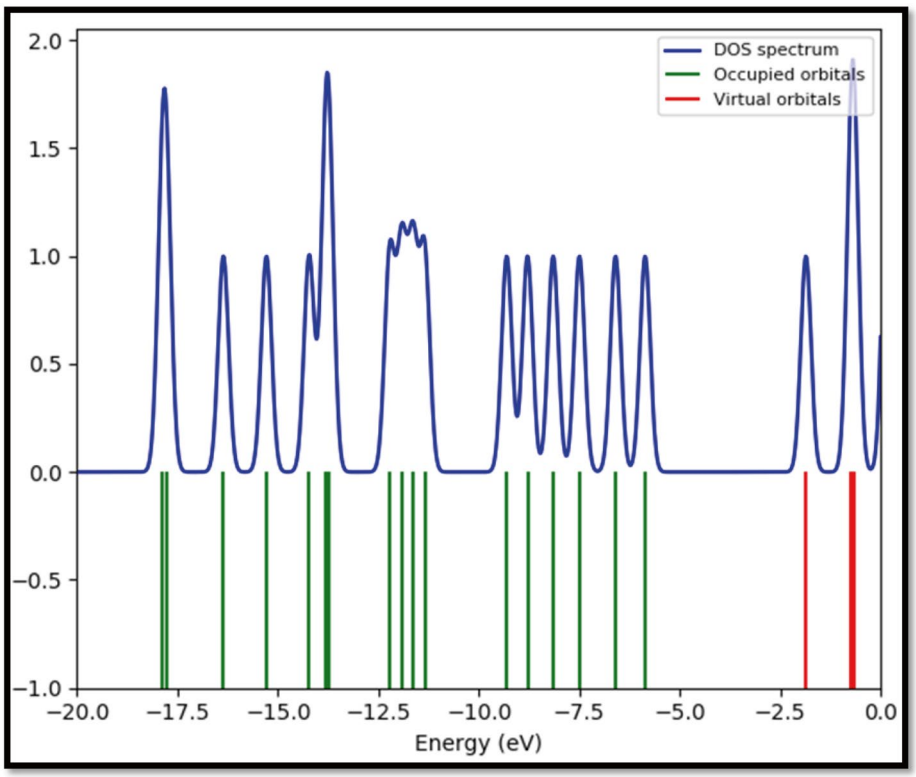

2O-s; $E_g = 4.00$ eV

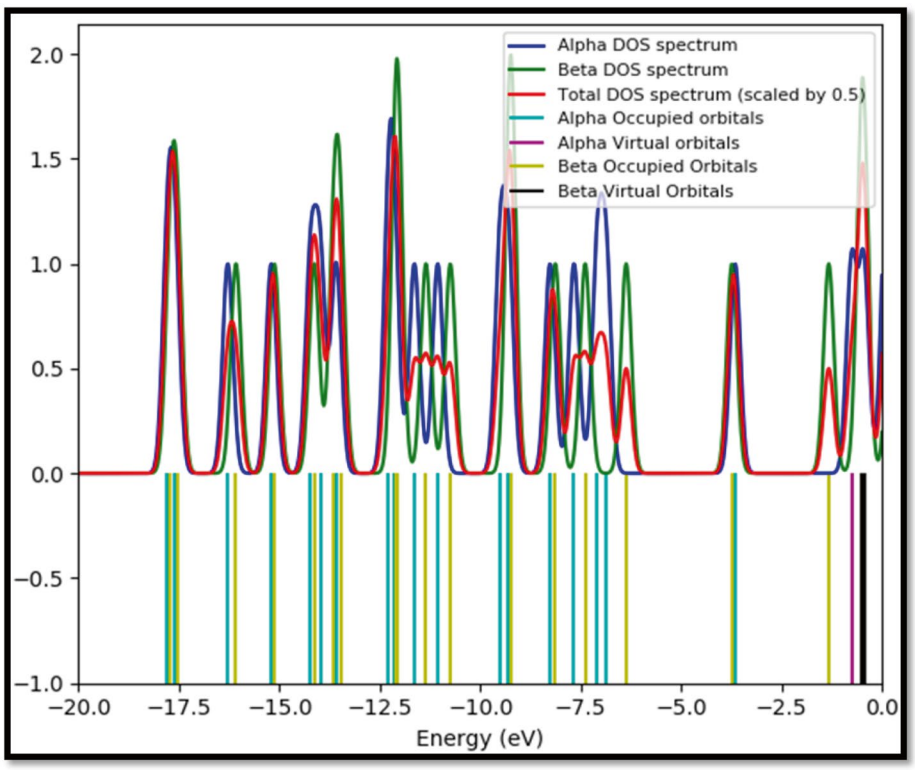

2O-t; $E_g = 2.56$ eV

Fig. 4 The density of state (DOS) plots of the selected **2O-s** and **2O-t** silylenes

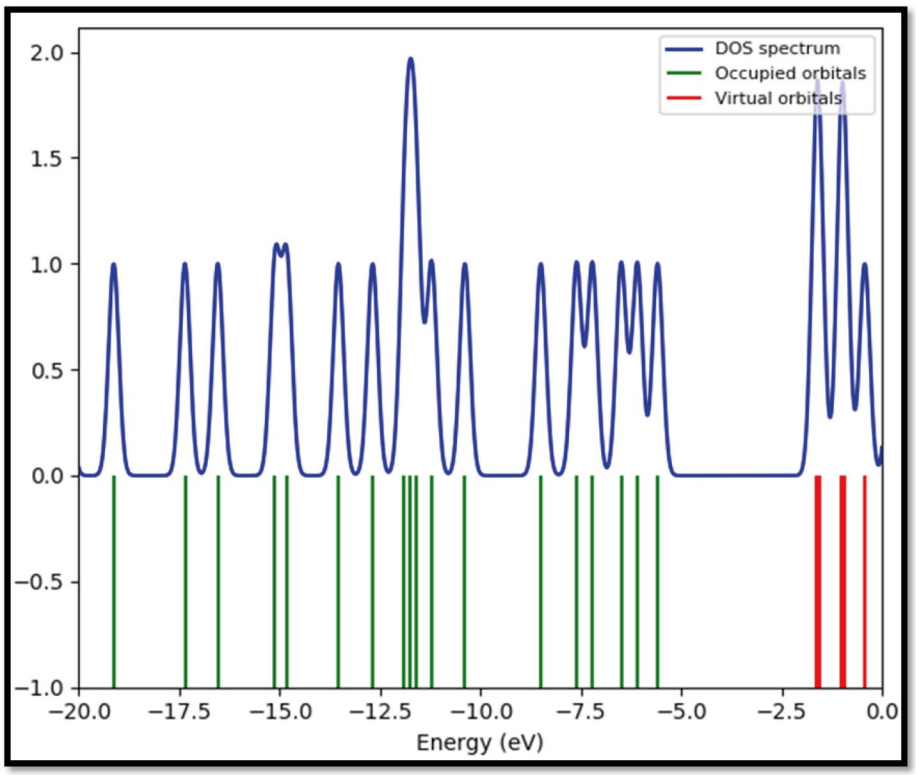

3AsH-s; E_g = 3.94 eV

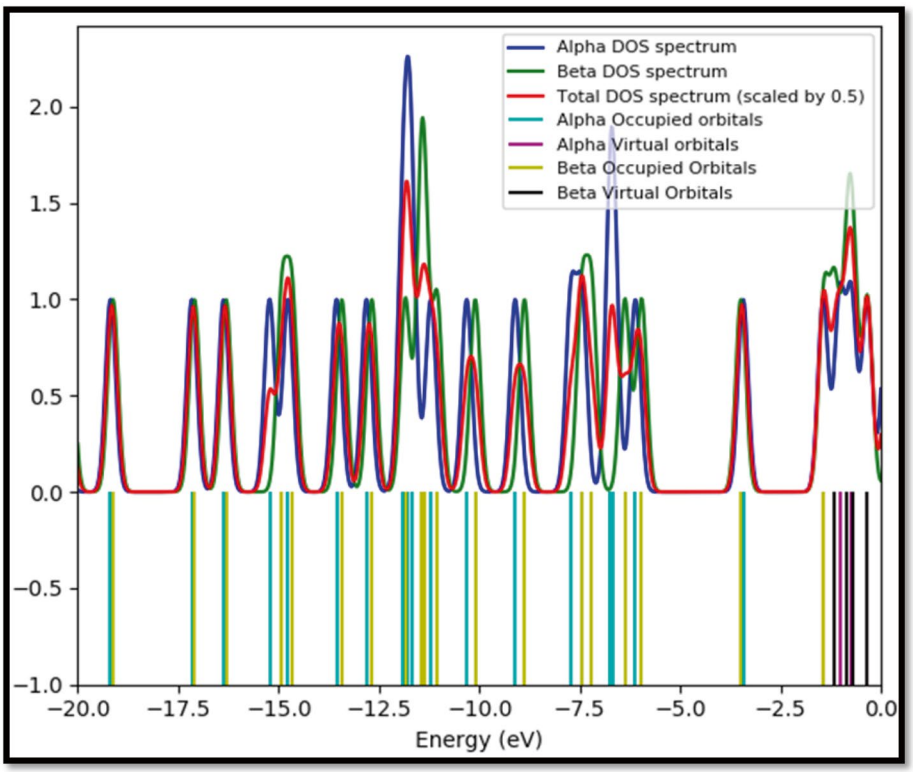

3AsH-t; E_g = 1.99 eV

Fig. 5 The DOS plots of the selected **3AsH-s** and **3AsH-t** silylenes

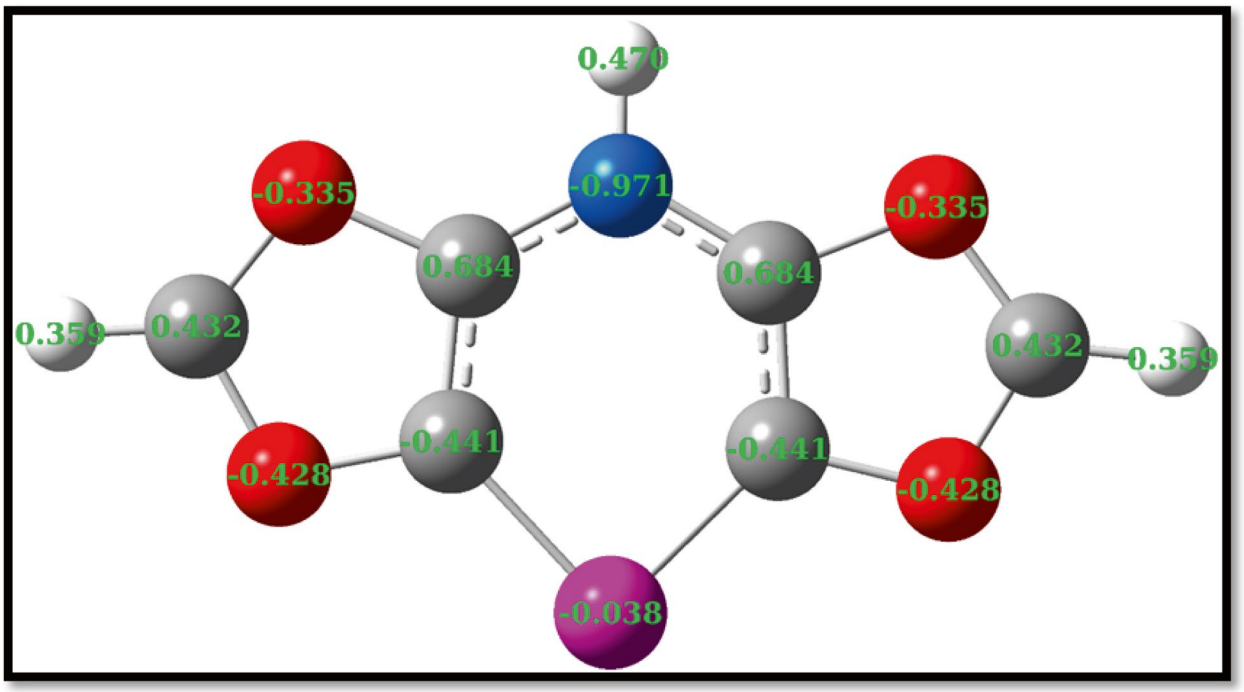

2O-s

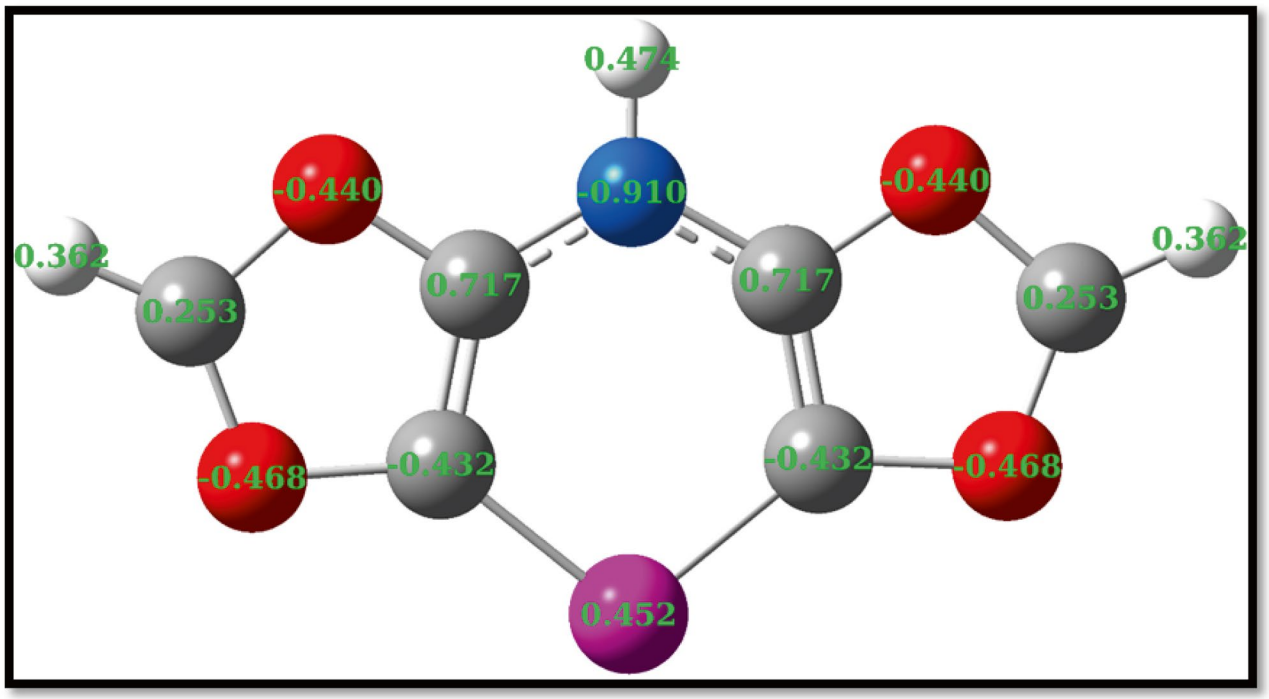

2O-t

Fig. 6 The NBO charges calculated for the selected **2O-s** and **2O-t** silylenes

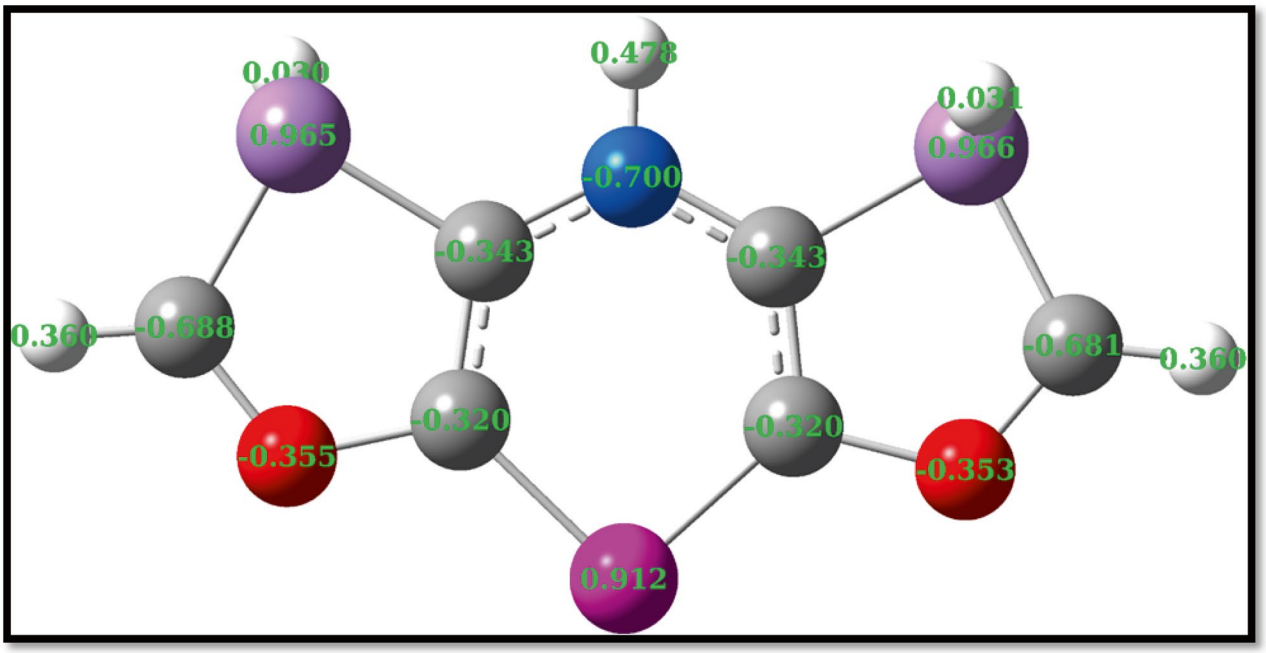

3AsH-s

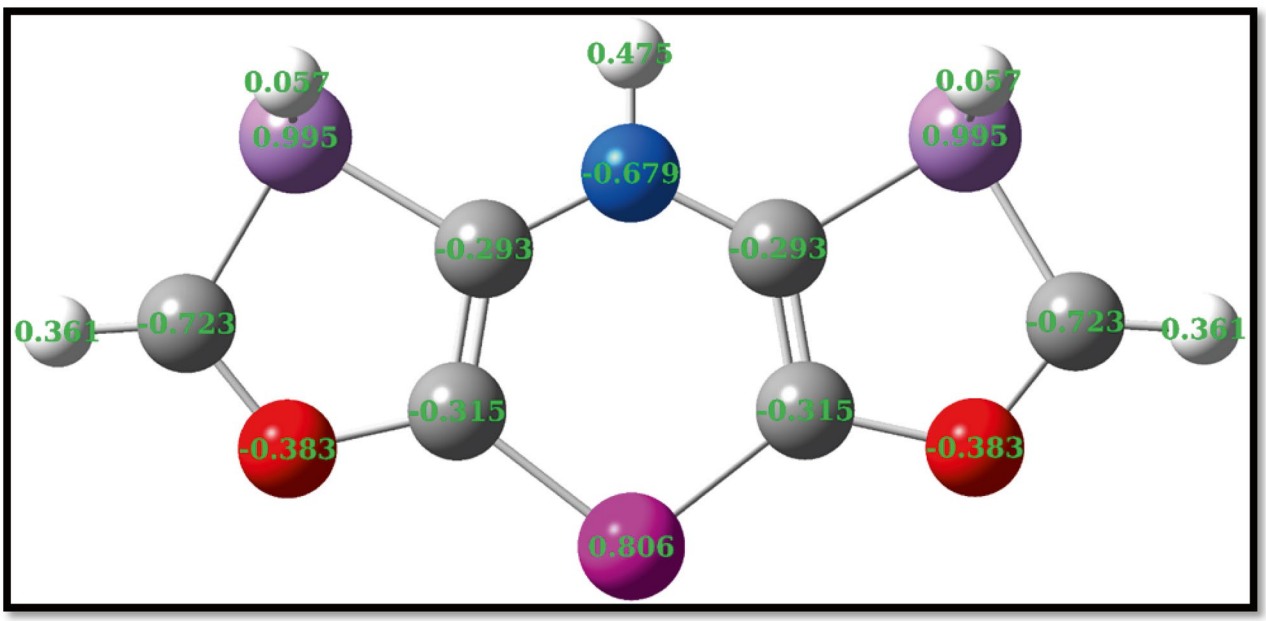

3AsH-t

Fig. 7 The NBO charges calculated for the selected **3AsH-s** and **3AsH-t** silylenes

Dissimilar to nonpolar and symmetric (achiral) molecules, the NBO charge is not commonly dispersed over the fused furan and silapyridine rings, revealing the inductive effect along with the mesomeric effect of the substituted EWGs and EDGs, respectively. For instance, we are shown the calculated NBO charges for the **2O-s**, **2O-t**, **3AsH-s**, and **3AsH-t** silylenes (Figs. 6 and 7).

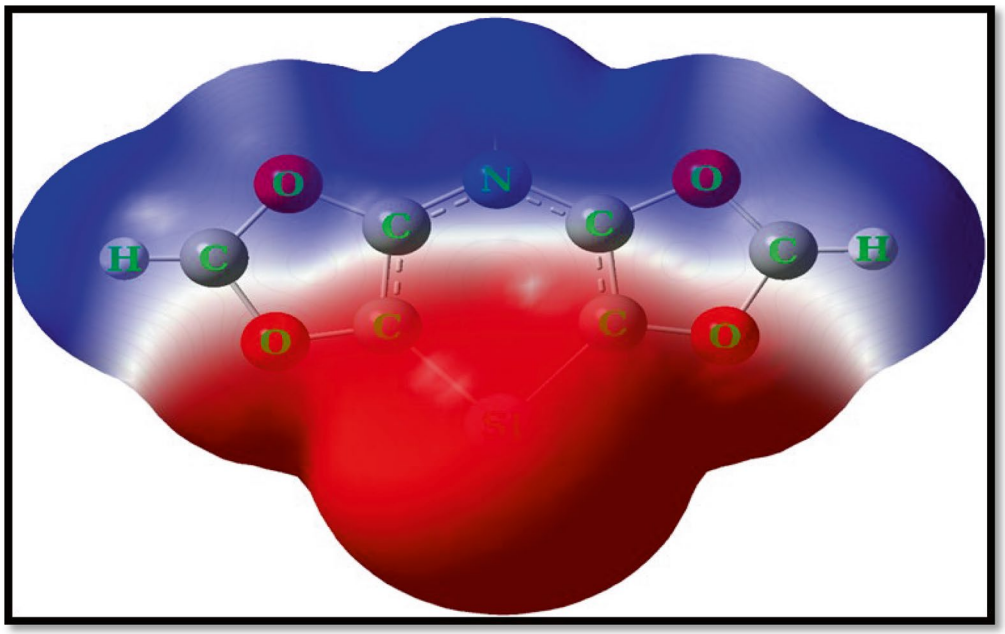

2O-t

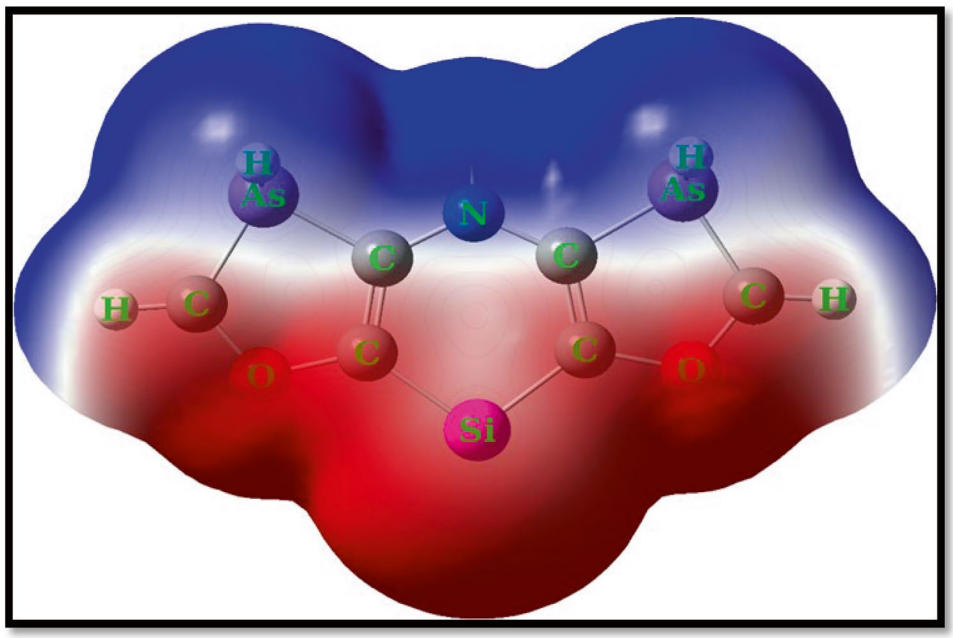

3AsH-t

Fig. 8 The ESP maps and contours of the selected **2O-t** and **3AsH-t** silylenes. The red and blue regions on the scale bar indicate the lowest and the highest ESP values, respectively

Table 3 The calculated N, ω, μ, η, S, and ΔN_{max} (all in kJ/mol) of the inspected singlet and triplet NHSis

Species	N	ω	μ	η	S	ΔN_{max}
1-s	391.35	156.15	−337.37	365.32	12.53	89.64
1-t	589.91	53.98	−177.36	290.14	16.39	58.80
2NH-s	354.72	164.83	−360.50	393.27	11.57	88.68
2NH-t	583.16	53.01	−178.32	299.78	15.42	57.83
2PH-s	354.72	173.50	−365.32	383.64	12.53	91.57
2PH-t	575.45	93.50	−213.99	244.83	19.28	83.86
2AsH-s	355.68	173.50	−365.32	383.64	12.53	91.57
2AsH-t	576.42	108.92	−221.70	226.52	20.24	94.46
2O-s	330.62	187.96	−384.60	393.27	11.57	94.46
2O-t	557.14	83.86	−215.92	277.61	16.39	75.18
2S-s	338.33	189.89	−381.71	384.60	12.53	95.43
2S-t	559.07	123.38	−238.09	230.37	20.24	99.28
2Se-s	342.19	188.93	−378.82	381.71	12.53	95.43
2Se-t	561.96	133.98	−240.98	216.88	21.21	106.99
3NH-s	373.03	153.26	−345.08	388.45	11.57	85.79
3NH-t	589.91	79.04	−198.57	247.72	18.31	77.11
3PH-s	374.00	160.97	−348.93	377.85	12.53	88.68
3PH-t	580.27	93.50	−212.06	239.05	19.28	84.82
3AsH-s	373.03	160.01	−348.93	379.78	12.53	88.68
3AsH-t	581.24	143.62	−235.19	191.82	24.10	118.56
3S-s	351.83	178.32	−369.18	382.67	12.53	92.54
3S-t	560.99	119.52	−235.19	231.34	20.24	98.32
3Se-s	354.72	174.47	−366.29	382.67	12.53	92.54
3Se-t	564.85	130.13	−238.09	217.84	21.21	105.07
I-s	385.56	100.25	−300.74	451.11	10.60	64.58
I-t	590.88	69.40	−189.89	261.22	17.35	70.37
II-s	415.44	91.57	−281.46	430.87	10.60	62.65
II-t	646.78	57.83	−158.08	214.95	21.21	70.37
III-s	376.89	184.11	−359.54	350.86	13.49	98.32
III-t	589.91	176.40	−253.51	137.84	33.74	176.40

Table 4 The calculated charges, CFF, and condensed dual descriptors for silylenic center of the selected singlet NHSis

	N	$N-1$	$N+1$	f^-	f^+	Df
1-s	0.246202	0.440159	0.071977	−0.1940	−0.1742	0.0197
2NH-s	−0.231504	0.157441	−0.355592	−0.3889	−0.1241	0.2649
2PH-s	−0.018365	0.267522	−0.213938	−0.2859	−0.1956	0.0903
2AsH-s	−0.017998	0.259987	−0.220018	−0.2780	−0.2020	0.0760
2O-s	0.056335	0.375183	−0.202857	−0.3188	−0.2592	0.0597
2S-s	0.137727	0.435282	−0.169472	−0.2976	−0.3072	−0.0096
2Se-s	0.056027	0.347627	−0.195511	−0.2916	−0.2515	0.0401
3NH-s	−0.06924	0.298285	−0.30532	−0.3675	−0.2361	0.1314
3PH-s	0.302538	0.464849	−0.198913	−0.1623	−0.5015	−0.3391
3AsH-s	0.297809	0.458859	−0.206562	−0.1611	−0.5044	−0.3433
3S-s	0.089755	0.410434	−0.196839	−0.3207	−0.2866	0.0341
3Se-s	0.056335	0.375183	−0.202857	−0.3188	−0.2592	0.0597

Table 5 The calculated E values for neutral (N), cation ($N-1$), and anion ($N+1$) states (in *hartree*), $IP = E_{(N-1)} - E_{(N)}$ and $EA = E_{(N+1)} - E_{(N)}$ (in kJ/mol) of the selected singlet NHSis

Species	$E_{(N)}$	$E_{(N-1)}$	$E_{(N+1)}$	IP	EA
1-s	−806.68	−806.416	−806.564	691.44	303.75
2NH-s	−835.35	−835.22	−835.35	361.00	9.86
2PH-s	−1408.44	−1408.25	−1408.41	387.73	−43.03
2AsH-s	−5193.04	−5192.87	−5193.07	445.90	−78.69
2O-s	−875.03	−874.87	−875.06	434.48	−84.35
2S-s	−1520.97	−1520.84	−1521.02	446.91	−110.81
2Se-s	−5523.38	−5523.22	−5523.42	422.58	−96.43
3NH-s	−835.35	−835.20	−835.33	387.90	50.49
3PH-s	−1408.47	−1408.29	−1408.54	485.59	−168.50
3AsH-s	−5193.33	−5193.12	−5193.37	476.89	−170.42
3S-s	−1520.96	−1520.79	−1521.01	448.49	−131.68
3Se-s	−5523.37	−5523.24	−5523.41	440.72	−94.34

Regardless of the W (zigzag) and/or chair arrangement, the positive NBO charge is dispersed over hydrogen, carbon, silylenic center, and EDGs, while the negative NBO charge is dispersed over silapyridinic's nitrogen, carbon, and EWGs. The dispersed NBO charge qualitatively confirms that the substituted EWGs and EDGs in the difuranosilapyridine structure either in the "W" or "chair" positions of the silylenic center stabilize not only the *s* NHSis but also the *t* ones. The negative and positive NBO charges of the *s* and *t* NHSis indicate that these sites can be attacked more easily by electrophilic and nucleophilic regents, correspondingly. The electrostatic potential (ESP) maps qualitatively confirm blue color for positive charge, red color for negative charge, the electron cloud in the middle of two rings, and the dependency of NBO charge on electronegativity of EWGs and EDGs (Fig. 8).

For enquiry of the substituent effects of EWGs and EDGs on global reactivity of their corresponding *s* and *t* NHSis, we are calculated N, ω, μ, η, S, and ΔN_{max} (Table 3).

A commonly found finding is the lower N, higher ω, higher absolute value of μ, higher η, and lower S of every *s* NHSis than every *t* congener. The positive ΔN_{max} index exhibits the positive charge capacity of every *s* and *t* NHSi, and here all species are expected electron acceptor in organic chemistry reactions or catalysts. Certainly, the five-membered furan ring contains lower basicity than the six-membered pyridine ring and other amines. The reduced basicity is strengthened by π-delocalization of the free electron on the oxygen atom of the furan ring. In fact, the smaller bond angle of the furan ring (about 12°) than the pyridine ring enlarges the *p* character of the bonding sp^2 orbital and the *s* character of the nonbonding σ orbital. Here, the higher *s* character of the nonbonding σ orbital of either the doped EWGs or EDGs in either W or chair positions leads to lower N and higher ω of their *s* and *t* NHSis than in **1-s** and **1-t** structures. The Hirshfield charges, CFFs, atomic, and global indices are calculated to predict the chemical system's reactive sites and character. Here, the Hirshfield charges, CFFs, and D*fs* for silylenic centers of the selected singlet NHSis display dissimilar trends dependent on the electronegativity, size, and topology of the substituted heteroatoms of NH, PH, AsH, O, S, and Se, either in the "W (*ortho*)" or "chair (*para*)" position of the silylenic center, in the fused rings (Table 4).

For example, the silylenic center of the **2NH-s** species shows the most nucleophilicity via the highest f^- (−0.3889 e), the lowest f^+ (−0.1241 e), and the most positive value of D*f* (+0.2649 e) between NHSis, while the silylenic center of the **3AsH-s** species shows the most electrophilicity via the lowest f^- (−0.1611 e), the highest f^+ (−0.5044 e), and the most negative value of D*f* (-0.3433 e) between NHSis. Comparatively, at the level of computation, the IP and EA for benzene (a reference molecule) have been reported to be 889.69 and −66.51 kJ/mol, respectively [90]. A closed look at **1-s** and the substituted NHSis (**2x-s** and **3x-s**) shows that the electrons are more and less binded than those of benzene, respectively (Table 5).

Interestingly, the **1-s** species shows the most positive value of IP and EA (691.44 and 303.75 kJ/mol), then the **2NH-s** and **3NH-s** isomers show the most positive value of IP and EA (361.00 and 50.49 kJ/mol, respectively), while the **3AsH-s** species shows the most negative value of EA (−170.42 kJ/mol) between NHSis. Hence, substituent effects compete with the aromaticity of NHSis because substituents' interaction with the π-system decreases degree the of π-electron delocalization.

Conclusion

To reach for novel *s* and *t* NHSis, we have studied electronic effects on structural, thermodynamic, and kinetic factors of the fused dibenzo and difuranosilapyridine-4-ylidenes. To this end, three series structures (from **1-s** to **3x-t**; x = NH, PH, AsH, O, S, and Se) are compared and contrasted with some of the synthesized silylenes using DFT. Every *s* NHSi exhibits more polarity, lower polarizability, more positive frequency, and higher $\Delta E_{HOMO\text{-}LUMO}$ than its corresponding *t* NHSi; yet $\Delta E_{HOMO\text{-}LUMO}$ of them is more than **III-s** and **III-t**. In other words, all silylenes substituted by EWGs and EDGs display more stability than **III,** so that the $\Delta E_{s\text{-}t}$ and $\Delta E_{HOMO\text{-}LUMO}$ ranges are changed from 193.66 and 379.50 kJ/mol for **3AsH** to 215.10 and 393.46 kJ/mol for **2O-s** vs. 138.48 and 351.33 kJ/mol for **III-s**, respectively. The ESP contour maps qualitatively confirm the distributed NBO atomic charge and determine nucleophilic and electrophilic sites. Moreover, *s* silylenes show lower nucleophilicity (N), higher electrophilicity (ω), chemical potential (μ), and global hardness (η) than their related *t* congeners. The fused furan NHSis (either

s or *t* ones) reveal lower *N* and higher ω than **1-s** and **1-t** structures on account of the inductive effect and mesomeric effect of the EWGs and EDGs on the completed σ^2 orbital and $3p_\pi^2$ orbital of their silylenic centers. Indeed, the stability and electronic properties of *s* and *t* NHSis are considerably dependent on the electronegativity and radius of the substituted groups. We hope for experimental investigations that substitute the different heteroatoms in two fused furan silapyridines either the "W" or "chair" position of the silylenic center with the purpose of stabilizing not only the *s* silylenes but also the *t* congeners. Based on the Hirshfield charge, CFF, and D*f* results, the silylenic center of the **2NH-s** species shows the highest nucleophilicity, whereas the silylenic center of the **3AsH-s** species shows the highest electrophilicity. A close look at **1-s** and the substituted NHSis (**2x-s** and **3x-s**) shows that the electrons are more and less binded than benzene.

Author contributions Marziyeh Mohammadi: Writing—review, editing, writing—original draft, project administration, investigation, visualization, methodology, formal analysis, data decoration, conceptualization, validation, software, resources, and project administration.

Data availability Not applicable.

Declarations

Competing interests The author declares no competing interests.

References

1. Koohi M (2019) Cyclonona-3,5,7-trienylidene and its Si, Ge, Sn, and Pb analogs versus their α-halogenated derivatives at B3LYP and MP2 methods. J Phys Org Chem 32:e4013
2. Koohi M (2020) Estimating the stability and reactivity of cyclic tetrahalo substituted germylenes: a density functional theory investigation. J Phys Org Chem 33:e4032
3. Koohi M, Bastami H (2020) A quest for stable 2,2,9,9-tetrahaloplumbacyclonona-3,5,7-trienylidenes at density functional theory. Struct Chem 31:877
4. Koohi M, Bastami H (2020) Substituent effects on stability, MEP, NBO analysis, and reactivity of 2,2,9,9-tetrahalosilacyclonona-3,5,7-trienylidenes, at density functional theory. Monatshefte für Chemie - Chemical Monthly 151:11
5. Koohi M, Bastami H (2020) A density functional theory perspective on 2,2,9,9-tetrahalostannacyclonona-3,5,7-trienylidenes. J Phys Org Chem 33:e4031
6. Koohi M, Bastami H (2020) Substituted Hammick carbenes: the effects of fused rings and hetero atoms through DFT calculations. J Phys Org Chem 33:e4023
7. Kassaee MZ, Koohi M (2013) Breathing viability into cyclonona-3,5,7-trienylidenes via a-dimethyl and ά-moieties at DFT. J Phys Org Chem 26:540
8. Kassaee MZ, Koohi M, Mohammadi R, Ghavami M (2013) 2,2,9,9-Tetramethylcyclonona-3,5,7-trienylidene *vs.* its heterocyclic analogues: a quest for stable carbenes at DFT. J Phys Org Chem 26:908
9. Koohi M, Kassaee MZ, Haerizade BN, Ghavami M, Ashenagar S (2015) Substituent effects on cyclonona-3,5,7-trienylidenes: a quest for stable carbenes at density functional theory level. J Phys Org Chem 28:514
10. Gehrhus B, Lappert MF, Heinicke J, Boese R, Bläser D (1995) Synthesis, structures and reactions of new thermally stable silylenes. J Chem Soc Chem Commun 0:1931
11. Heinicke J, Oprea A, Kindermann MK, Karpati T, Nyulaszi L, Veszpremi T, Hitchcock PB, Lappert MF, Maciejewski H (1998) Silylenenickel(0) or silyl(silylene)platinum(II) complexes by reaction of $Si[(NCH_2Bu^t)_2C_6H_4–1,2]$ with $[NiCl_2(PPh_3)_2]$, $[Ni(cod)_2]$, or $[PtCl_2(PPh_3)_2]$. Organomet 17:5599
12. Becerra R, Walsh R (2010) Dalt Trans 39:9217
13. Kassaee MZ, Zandi H, Haerizade BN, Ghambarian M (2012) Effects of α-mono heteroatoms (N *vs.* P), and β-conjugation on cyclic silylenes. Comput Theor Chem 1001:39
14. Ayoubi-Chianeh M, Kassaee MZ, Ashenagar S, Cummings PT (2019) Nucleophilicity of cyclic conjugated silylenes using DFT method. J Phys Org Chem 32:ee3956
15. Cote DR, Van Nguyen S, Stamper AK, Armbrust DS, Tobben D, Conti RA, Lee GY (1999) Plasma-assisted chemical vapor deposition of dielectric thin films for ULSI semiconductor circuits. IBM J Res Dev 43(1.2):5
16. Hopkinson AC, Lien MH, Csizmadia LG (1983) Ab initio calculations on the singlet and triplet energy surfaces for $CsiH_2$. Chem Phys Lett 95:232
17. Gordon MS, Pople JA (1981) Structure and stability of a silicon-carbon triple bond. J Am Chem Soc 103:2945
18. Gordon MS (1982) Effects of polar substituents on carbon-silicon multiple bonds. J Am Chem Soc 104:4352
19. Luke BT, Pople JA, Krogh-Jespersen M-B, Apeloig Y, Karni M, Chandrasekhar J, Schleyer PVR (1986) A theoretical survey of unsaturated or multiply bonded and divalent silicon compounds. Comparison with carbon analogs. J Am Chem Soc 108(2):270
20. Kosa M, Karni M, Apeloig Y (2013) Were reactions of triplet silylenes observed? J Am Chem Soc 135(24):9032
21. Murrell JN, Kroto HW, Guest MF (1977) Double-bonded divalent silicon: *ab-initio* calculations on the species HSiN, HNSi, HCSiH, and H_2CSi. J Chem Soc Chem Commun 17:619
22. Leclercq H, Dubois I (1979) The absorption spectrum of the H_2CSi radical. J Mol Spectrosc 76(1–3):39
23. Izuha M, Yamamoto S, Saito S (1996) Microwave spectrum of silylidene H_2CSi. J Chem Phys 105:4923
24. Smith TC, Evans CJ, Clouthier DJ (2003) Discovery of the optically forbidden S_1–S_0 transition of silylidene ($H_2C{=}Si$). J Chem Phys 118:1642
25. Sherrill CD, Schaefer HF III (1995) 1-silavinylidene: the first unsaturated silylene. J Phys Chem 99:1949
26. Hoffmann MR, Yoshioka Y, Schaefer HF III (1983) Vibrational frequencies for silaacetylene and its silylidene and vinylidene isomers. J Am Chem Soc 105:1084
27. Sharma M, Sharma MK, Verma UP, Chandra S (2014) Radiative transfer in silylidene molecule. Serbian Astron J 2014:37
28. Harper WW, Ferrall EA, Hilliard RK, Stogner SM, Grev RS, Clouthier DJ (1997) Laser spectroscopic detection of the simplest unsaturated silylene and germylene. J Am Chem Soc 119(35):8361
29. Bourissou D, Guerret O, Gabbai FP, Bertrand G (2000) Stable carbenes. Chem Rev 100:39
30. Gordon MS (1985) Potential-energy surfaces in singlet and triplet silylene. Chem Phys Lett 114:348
31. Holthausen MC, Koch W, Apeloig Y (1999) Theory predicts triplet ground-state organic silylenes. J Am Chem Soc 121(11):2623
32. Nemirowski A, Schreiner PR (2007) Electronic stabilization of ground state triplet carbenes. J Org Chem 72(25):9533
33. Dubois I, Herzberg G, Verma RD (1967) Spectrum of SiH_2. J Chem Phys 47(10):4262

34. Ghaghaei M, Babazadeh M, Behmagham F, Edjlali L, Vessally E (2023) A theoretical evaluation for new fused remote N-heterocyclic silylenes (RNHSis) using density functional theory. J Phys Org Chem 16(7):e4475. https://doi.org/10.1002/poc.4475
35. Zhao H, Yang D, Zhou Y, Fang Y, Shi M, Vessally E (2020) A computational quest for the effects of fused rings on the stability of Hammick carbenes type remote N-heterocyclic carbenes. J Chin Chem Soc 68:76
36. Delir Kheirollahi Nezhad P, Youseftabar-Miri L, Ahmadi S, Ebrahimiasl S, Vessally E (2021) A DFT quest for effects of fused rings on the stability of remote *N*-heterocyclic carbenes. Struct Chem 32:787
37. Hassanpour A, Poor Heravi MR, Rahmani Z, Ebadi AG, Ahmadi S (2021) Characterization of novel pyridine-derived N-heterocyclic silylenes via density functional theory perspective. J Chin Chem Soc 68:1405
38. Söğütlü İ, Soltanzadeh M, Mert H, Mert N, Vessally E (2021) Substituent effects on the stability of cyclic - unsaturated remote *N*-heterocyclic Hammick carbenes using density functional theory. J Mol Struct 1230:129821
39. Zhao K, Zhang Y, Ma Y, Jin Z, Rashid Sheykhahmad F (2020) Stabilization of novel *N*-heterocyclic Germylenes (NHGes): a computational perspective. J Chin Chem Soc 68:274
40. Schmidt MW, Baldridge KK, Boatz JA, Elbert ST, Gordon MS, Jensen JH, Koseki S, Matsunaga N, Nguyen KA, Su SJ, Windus TL, Dupuis M, Montgomery JA (1993) General atomic and molecular electronic structure system. J Comput Chem 14(11):1347
41. Sobolewski AL, Domcke W (2002) *Ab initio* investigation of the structure and spectroscopy of hydronium−water clusters. J Phys Chem A 106:4158
42. Becke AD (1988) Density-functional exchange-energy approximation with correct asymptotic behavior. Phys Rev A 38:3098
43. Becke AD (1993) Density-functional thermochemistry. III. The role of exact exchange. J Chem Phys 98:5648
44. Becke AD (1996) Density-functional thermochemistry. IV. A new dynamical correlation functional and implications for exact-exchange mixing. J Chem Phys 104:1040
45. Lee C, Yang W, Parr RG (1988) Development of the Colle-Salvetti correlation-energy formula into a functional of the electron density. Phys Rev B 37:785
46. Zhao Y, Truhlar DG (2008) Density functionals with broad applicability in chemistry. Acc Chem Res 41(2):157
47. Zhao Y, Truhlar DG (2008) The M06 suite of density functionals for main group thermochemistry, thermochemical kinetics, noncovalent interactions, excited states, and transition elements: two new functionals and systematic testing of four M06-class functionals and 12 other functionals. Theor Chem Account 120:215
48. Hariharan PC, Pople JA (1974) Accuracy of AH, equilibrium geometries by single determinant molecular orbital theory. J Mod Phys 27:209
49. Francl MM, Pietro WJ, Hehre WJ, Binkley JS, Gordon MS, DeFrees DJ, Pople JA (1982) Self-consistent molecular orbital methods. XXIII. A polarization-type basis set for second row elements. J Chem Phys 77:3654
50. Clark T, Chandrasekhar J, Spitznagel GW, Schleyer PVR (1983) Efficient diffuse function-augmented basis sets for anion calculations. III. The 3–21+G set for first-row elements, Li-F. J Comput Chem 4:294
51. Frisch MJ, Pople JA, Binkley JS (1984) Self-consistent molecular orbital methods 25: supplementary functions for Gaussian basis sets. J Chem Phys 80:3265
52. Hehre WJ, Radom L, PvR S, Pople JA (1986) *Ab initio* molecular orbital theory. John Wiley & Sons, New York
53. Foresman JB, Frisch A (1996) Exploring chemistry with electronic structure methods, Gaussian, Inc., Pittsburgh. PA
54. Kendall RA, Dunning TH Jr, Harrison RJ (1992) Electron affinities of the first-row atoms revisited. Systematic basis sets and wave functions. J Chem Phys 96:6796
55. Krishna R, Frisch MJ, Pople JA (1980) Contribution of triple substitutions to the electron correlation energy in fourth order perturbation theory. J Chem Phys 72:4244
56. Weinhold F, Glendening ED (2001) NBO 7.0 Program Manual Natural Bond Orbital Analysis Programs
57. Weinhold F (2012) Natural Bond Orbital Analysis: A Critical Overview of Relationships to Alternative Bonding Perspectives. J Comput Chem 33:2363
58. Glendening ED, Landis CR, Weinhold F (2012) Natural bond orbital methods. Wiley Interdiscip Rev Comput Mol Sci 2:1
59. Zhang G, Musgrave CB (2007) Comparison of DFT Methods for Molecular Orbital Eigenvalue Calculations. J Phys Chem A 111:1554
60. Gharibzadeh F, Vessally E, Edjlali L, Es'haghi M, Mohammadi R (2020) A DFT study on sumanene, corannulene and nanosheet as the anodes in Li−ion batteries. Iran J Chem Chem Eng 39:51
61. Afshar M, Khojasteh RR, Ahmadi R, Nakhaei Moghaddam M (2021) In silico adsorption of lomustin anticancer drug on the surface of boron nitride nanotube. Chem Rev Lett 4:178
62. Vessally E, Hosseinian A (2021) A computational study on the some small graphene-like nanostructures as the anodes in Na−ion batteries. Iran J Chem Chem Eng 40:691
63. Hashemzadeh B, Edjlali L, Delir Kheirollahi Nezhad P, Vessally E (2021) A DFT studies on a potential anode compound for Li-ion batteries: hexa-cata-hexabenzocoronene nanographen. Chem Rev Lett 4:232
64. Vessally E, Farajzadeh P, Najafi E (2021) Possible sensing ability of boron nitride nanosheet and its Al– and Si–doped derivatives for methimazole drug by computational study. Iran J Chem Chem Eng 40:1001
65. Cao Y, Rostami Z, Ahmadi R, Azimi SB, Nayini MMR, Ansari MJ (2022) Study the role of MgONTs on adsorption and detection of carbon dioxide: First-principles density calculations. Comput Theor Chem 1208:113572
66. Salehi N, Vessally E, Edjlali L, Alkorta I, Eshaghi M (2020) Nan@Tetracyanoethylene (n=1-4) systems: sodium salt vs sodium electride. Chem Rev Lett 3:207
67. Soleimani-Amiri S, Asadbeigi N, Badragheh S (2020) A theoretical approach to new triplet and quintet (nitrenoethynyl) alkylmeth ylenes,(nitrenoethynyl) alkylsilylenes, (nitrenoethynyl) alkylgermylenes. Iran J Chem Chem Eng (IJCCE) 39(4):39
68. Arshadi S, Abdolahzadeh F, Vessally E (2023) Butadiyne-linked porphyrin nanoring as a highly selective O_2 gas sensor: A fast response hybrid sensor. J Mol Graph Model 119:108371
69. Khalif M, Daneshmehr S, Arshadi S, Söğütlü İ, Mahmood EA, Abbasi V, Vessally E (2023) Adsorption of O_2 molecule on the transition metals (TM (II)= Sc^{2+}, Ti^{2+}, V^{2+}, Cr^{2+}, Mn^{2+}, Fe^{2+}, Co^{2+}, Ni^{2+}, Cu^{2+} and Zn^{2+}) porphyrins induced carbon nanocone (TM (II) PCNC). J Mol Graph Model 119:108362.
70. Kamel M, Mohammadifard M (2021) Thermodynamic and reactivity descriptors Studies on the interaction of flutamide anticancer drug with nucleobases: a computational view. Chem Rev Lett 4:54
71. Vessally E, Musavi M, Poor Heravi MR (2021) A density functional theory study of adsorption ethionamide on the surface of the pristine, Si and Ga and Al-doped graphene. Iran J Chem Chem Eng (IJCCE) 40:1720
72. Vakili M, Bahramzadeh V, Vakili M (2020) A Comparative study of SCN- adsorption on the $Al_{12}N_{12}$, $Al_{12}P_{12}$, and Si and Ge -doped $Al_{12}N_{12}$ nano-cages to remove from the environment. J Chem Lett 1:172
73. SÖĞÜTLÜ İ, Arshadi S, Mahmood EA, Abbasi V, Kamalinahad S, Vessally E (2023) In silico investigation of metalophthalocyanine substituted in carbon nanocones (TM-PhCCNC, TM= Sc^{2+},

Cr^{2+}, Fe^{2+} and Zn^{2+}) as a promising sensor for detecting N2O gas involved. J Mol Struc 135263. https://doi.org/10.1016/j.molstruc.2023.135263
74. Mosavi M (2020) Adsorption behavior of mephentermine on the pristine and Si, Al, Ga- doped boron nitride nanosheets: DFT studies. J Chem Lett 1:164
75. Vessally E, Siadati SA, Hosseinian A, Edjlali L (2017) Selective sensing of ozone and the chemically active gaseous species of the troposphere by using the C_{20} fullerene and graphene segment. Talanta 162:505
76. Kadhim MM, Mahmood EA, Abbasi V, Heravi MRP, Habibzadeh S, Mohammadi-Aghdam S, Soleimani-Amiri S (2023) Investigation of the substituted—Titanium nanocages using computational chemistry. J Mol Graph Model 118:108317
77. Jalali Sarvestani MR (2022) Venlafaxine Interaction with Fullerene (C20): DFT Studies. J Chem Lett 3:169
78. Siadati SA, Vessally E, Hosseinian A, Edjlali L (2016) Possibility of sensing, adsorbing, and destructing the Tabun-2D-skeletal (Tabun nerve agent) by C_{20} fullerene and its boron and nitrogen doped derivatives. Synth Met 220:606
79. Kadhim MM, Mahmood EA, Abbasi V, Heravi MRP, Habibzadeh S, Mohammadi-Aghdam S, Shoaei SM (2022) Theoretical investigation of the titanium—nitrogen heterofullerenes evolved from the smallest fullerene. J Mol Graph Model 117:108269
80. Domingo LR, Chamorro E, Pérez P (2008) Understanding the reactivity of captodative ethylenes in polar cycloaddition reactions. A theoretical study J Org Chem 73:4615
81. Parr RG, Pearson RG (1983) Absolute hardness: companion parameter to absolute electronegativity. J Am Chem Soc 105:7512
82. Parr RG, Yang W (1989) Density functional theory of atoms and molecules. Oxford University Press, New York
83. Parr RG, Szentpaly L, Liu S (1999) Electrophilicity Index. J Am Chem Soc 121:1922
84. Wang B, Rong C, Chattaraj PK, Liu S (2019) A comparative study to predict regioselectivity, electrophilicity and nucleophilicity with Fukui function and Hirshfeld charge. Theor Chem Account 138(12):124
85. Agwupuye JA, Louis H, Enudi OC, Unimuke TO, Edim MM (2022) Theoretical insight into electronic and molecular properties of halogenated (F, Cl, Br) and hetero-atom (N, O, S) doped cyclooctane. Mater Chem Phys 275:125239
86. West R, Denk M (1996) Stable silylenes: synthesis, structure, reactions. Pure Appl Chem 68(4):785
87. Driess M, Yao S, Brym M, Cv W, Lentz D (2006) A new type of N-heterocyclic silylene with ambivalent reactivity. J Am Chem Soc 128(30):9628
88. Kira M, Ishida S, Iwamoto T, Kabuto C (1999) The first isolable Dialkylsilylene. J Am Chem Soc 121:9722
89. Hoffmann R, PvR S, Schaefer HF (2008) Predicting molecules—more realism, please! Angew Chem Int Ed 47:7164
90. Ebbesen TW (2016) Hybrid light–matter states in a molecular and material science perspective. Acc Chem Res 49(11):2403